Available online at www.sciencedirect.com
ScienceDirect
Nuclear Instruments and Methods in Physics Research A 584 (2008) 383–400
NUCLEAR INSTRUMENTS & METHODS IN PHYSICS RESEARCH Section A
www.elsevier.com/locate/nima

# Passive neutron detection for interdiction of nuclear material at borders

Richard T. Kouzes*, Edward R. Siciliano, James H. Ely, Paul E. Keller, Ronald J. McConn

*Pacific Northwest National Laboratory, MS K7-36, P.O. Box 999, Richland, WA 99352, USA*

Received 9 April 2007; received in revised form 9 October 2007; accepted 15 October 2007
Available online 22 October 2007

**Abstract**

Radiation portal monitor systems based upon polyvinyl toluene scintillator gamma-ray detectors and pressurized $^{3}$He-based neutron detector tubes have been deployed to detect illicit trafficking in radioactive materials at international border crossings. This paper reviews the neutron detection requirements and capabilities of passive, as opposed to active interrogation, detection systems used for screening of high-volume commerce for illicit sources of radiation at international border crossings. Computational results are given for the impact of cargo materials on neutron spectra, for the response of various detector geometries, the effects of backgrounds including "ship effect" neutrons, and for simulation of a large neutron detection array.


*PACS:* 29-40.−n

*Keywords:* Neutron detection; Ship effect; Portal monitor; Radiation detection; Homeland security; Border security; Detection of illicit materials; Monte Carlo modeling

## 1. Introduction

Radiation portal monitor (RPM) systems have been deployed to detect illicit trafficking in radioactive materials at international border crossings over the last several years [1]. Such systems have also long been used for safeguards applications [2] and for screening of scrap metal [3]. These large, passive detection systems are currently based upon panels of polyvinyl toluene plastic scintillator for gamma-ray detection and pressurized $^{3}$He-based neutron detector tubes. Radiation alarm algorithms used in such systems are typically based upon the net-counts above background observed in the gamma-ray or neutron detectors. Much of the published information on radiation detection for interdiction, and the research being performed, has centered upon the gamma-ray detection aspects of these systems, since gamma rays are produced by all of the sources of concern for illicit trafficking [4,5].

Sources of most concern include: complete weapons of mass destruction (WMD); improvised nuclear devices (IND); special nuclear material (SNM) for weapons construction, including plutonium and highly enriched uranium (HEU); and material or assemblies for radiological dispersal devices (RDD), also known as dirty bombs. All of these radioactive materials produce a gamma radiation signature, while plutonium, unique in its role as part of a weapon of mass destruction, also emits significant neutron radiation. Of these threats, HEU is perhaps the most difficult to detect because the gamma rays are of low energy, and thus, easily shielded; HEU has a very low emission rate of neutrons.

Detection of these threats through their gamma-ray signatures can be limited by a number of factors, including the high level and variability of natural background, the presence of naturally occurring radioactive material (NORM) in commerce [6,7], the presence of individuals with radionuclide burdens from medical treatments [8], and the impact of cargo on the background environment observed by these detectors [9]. Neutron detection has the advantages of a low natural background, few neutron sources being carried in the normal flow of commerce, and

*Corresponding author. Tel.: +1 509 372 4858; fax: +1 509 372 4969.
*E-mail addresses:* richard.kouzes@pnl.gov, rkouzes@pnl.gov (R.T. Kouzes).

0168-9002/$ - see front matter © 2007 Elsevier B.V. All rights reserved.
doi:10.1016/j.nima.2007.10.026

different shielding characteristics compared to gamma rays as will be discussed in detail in subsequent sections.

Given the need to interdict such threat sources, the issue addressed in this paper is how best to utilize neutron detection to complement gamma-ray detection. A number of authors have reported on research efforts on active interrogation methodologies where neutron or gamma-ray sources are used to stimulate neutron or gamma-ray responses from threat items hidden in cargo [11–15]. Such active interrogation systems are not considered here. This paper focuses only on passive detection of neutrons, such as that currently implemented in deployed RPM interdiction systems at US and foreign borders. More complex passive techniques such as coincidence counting are not considered.

The material presented below begins with a discussion of neutron sources and how neutrons are currently detected by RPMs. This is followed by a discussion of backgrounds and how these play into nuisance alarms for deployed systems. These sections serve as a backdrop for the subsequent discussion on how to detect radiological threats. To better understand how neutrons interact with instruments, results are discussed from simulations of neutron sources and detectors, ending with a proposed new detector array for which these insights are utilized.

## 2. Neutron sources

Many commercial neutron sources are made by mixing an alpha producing isotope with a material that contains an element with high probability for an (α,n) reaction. Beryllium has the highest probability for producing neutrons via this reaction, and is the most commonly used material in conjunction with an alpha source. Lithium is another choice for target material, and is used when low-energy neutrons are required. If an actinide is used for the alpha source and beryllium for the target element, a stable alloy is usually made from the two metals so that the alpha emitter (actinide) and the target (beryllium) are homogeneously distributed. Actinides that have reasonably long half-lives and do not also produce large fluxes of gamma rays are plutonium (both $^{238}$Pu and $^{239}$Pu isotopes), americium ($^{241}$Am), and curium ($^{244}$Cm). When combined in this fashion, the sources are usually abbreviated with the element symbol, e.g., a plutonium–beryllium source is referred to as PuBe. Other common sources are americium–beryllium (AmBe) and americium–lithium (AmLi). The PuBe source using $^{239}$Pu is perhaps the most common one, but higher neutron yields for a fixed mass can be obtained with the other actinide choices.

A small number of neutron sources are found in the normal flow of commerce, far smaller than the number of gamma-ray emitting sources. Among these neutron sources are those used for soil and concrete moisture measurements (such as those manufactured by Troxler Electronic Laboratories, Inc., Research Triangle Park, NC) and for the examination of oil and gas wells (“well logging” sources). Neutron sources including $^{241}$AmBe, $^{209}$PoBe, $^{239}$PuBe, $^{226}$RaBe, and spontaneous fission sources like $^{252}$Cf, are used for these and other commercial and scientific applications, accounting for their presence in commerce. Spontaneous fission sources, like $^{252}$Cf, have a neutron energy spectrum that is very similar to that from plutonium (i.e., spontaneous fission from $^{240}$Pu and induced fission in $^{239}$Pu), and are thus used as surrogate sources for instrument testing. The form of the source (metal or oxide) and surrounding matrix and shielding materials impact the energy spectrum and flux that is observed by a detection system. While a $^{252}$Cf neutron source has a relatively short half-life (2.6 yr), the (α,n) sources can have much longer half-lives. However, the neutron energy spectra from (α,n) sources are not good matches to the Pu fission spectra of greatest interest.

Depleted uranium (DU), a minor source of neutrons even when present in large quantities, is used for the construction of shipping casks, military armor, and aircraft counterweights, among other uses. Commercial shipments of large masses of natural or enriched uranium oxide or uranium hexafluoride are associated with the nuclear power industry and can produce significant numbers of neutrons. For example, a typical shipment of nuclear fuel might contain 2700 kg of natural or low enrichment uranium and emit over 37 000 neutrons/s. This flux is somewhat enhanced over what would come from a metallic source due to (α,n) reactions on the oxygen or other elements in or around the fuel.

Energy spectra for fission-produced neutrons from $^{252}$Cf and (α,n) reaction-produced neutrons for unmoderated sources from a number of standard references are shown as lethargy plots in Fig. 1 (data from Refs. [16,17,19,20,21]). These lethargy plots are histograms that have a horizontal logarithmic energy axis, while the vertical axis is the number of counts normalized by the logarithm of the

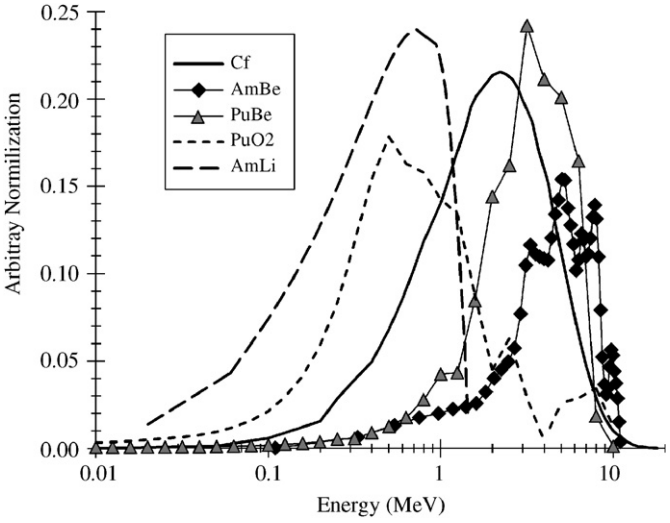


Fig. 1. Lethargy plots of energy spectra of several neutron sources. AmLi data are from Ref. [16]. AmBe and $^{252}$Cf data are from Ref. [17]. $PuO_2$ data are from Ref. [18] and [19]. PuBe data are from Refs. [20,21].

energy range of each bin. This has the advantage of providing a picture that shows visually accurate area plots. For the purpose of this figure, the neutron data from each of these different measurements have been renormalized to display their distributions on the same vertical axis over the energy range covered.

The fission produced neutron spectra shown are very similar in the region of energy near their maxima (~900 keV), but decrease at very different rates for energies below ~100 keV. In contrast, the (α,n) spectra from the different target elements have significantly different peak positions due to the different reaction $Q$-values, e.g., the AmLi source has more low-energy neutrons compared to the fission sources, while the AmBe source has more high-energy neutrons. The neutron energy spectrum for any actinide mixed with beryllium is similar, and for clarity only AmBe and PuBe are shown, which can be seen to be similar. This would also be true for (α,n) reactions arising from U emissions since all alphas are predominantly emitted with energies in the 4–5 MeV region. An (α,n) reaction on F would produce a spectrum close to that from Li. This reflects the (α,n) reaction $Q$-values of 5.71 MeV for Be, −2.79 MeV for Li, and −1.93 MeV for F. Fluorine is the source for (α,n) neutrons from $UF_6$ that is commonly shipped for the production of nuclear fuel. The spectrum shown for $PuO_2$ includes fission neutrons plus those from (α,n) reactions on O, giving it a different shape than the pure fission spectrum of $^{252}$Cf.

A characteristic feature of neutron sources in commerce is that they are point-like as opposed to distributed sources like many gamma-ray emitting NORM loads. An unshielded point source, whether gamma or neutron, produces a "Gaussian-like" profile in time as it passes a detector at a constant speed that is governed by the solid angle subtended by the area of the detector (see Ref. [22] for a discussion of the distribution). However, a point gamma-ray source within a cargo-filled container will typically give a narrower distribution than a point neutron source due to scattering in the cargo and the lower effectiveness of cargo shielding on the neutrons. In addition, due to the large field of view and consequently poor spatial resolution of typical RPM detectors, even point sources (neutron or gamma) may be indistinguishable from pallet-sized sources. For these reasons, spatial information may be useful, but not definitive, in differentiating point sources from distributed sources.

As a final point in this discussion of the general characteristics of neutron sources of interest, it is reasonable to assume that any illicit threat source will be shielded to reduce the probability of detection. Since the materials that are effective for shielding of gamma rays (high atomic number elements) are different from those that are effective for shielding of neutrons (low atomic number elements), a shield around the source designed to prevent the detection of gamma rays may not be effective for neutrons, and vice versa. An engineered shield to attenuate both would tend to be large and thus might easily be observable in the X-ray imaging that plays a complementary role to passive radiation detection for border interdiction applications.

## 3. Neutron detectors

Neutrons may be detected from the observation of the effects of recoiling protons resulting from collisions, or from the gamma rays and particles that may be released after the neutron is captured by a nucleus. The detectors often used in neutron instruments are more sensitive to very low-energy neutrons, and these detectors are generally surrounded by several centimeters of a hydrogenous moderator, such as polyethylene, that has a high proton density. The moderator slows the neutrons to increase their detection probability in the detector. Background information on neutron detection may be found in the textbook by Knoll [23], and recent developments are reviewed by Peurrung [24]. Neutron detectors continue to evolve, as exemplified by recent work on organic scintillators [25] and on $^6$LiI scintillators [26].

A number of detector materials, such as $^6$LiI or $^3$He, have large low-energy neutron cross-sections that vary inversely with the neutron velocity. The high sensitivity of detectors based on these materials to slow neutrons can be advantageous since the lower energy neutrons may more likely be encountered in the search for illicit sources due to moderation from cargo. Sensitivity to fast neutrons is also needed since unmoderated neutrons may also be encountered. The $^3$He-filled proportional counter encased by a polyethylene moderator is the most common neutron detector used in RPMs because, if designed with appropriate amounts of surrounding moderator, these sensors can achieve good intrinsic detection efficiency over the entire incident neutron energy range. Such detectors are available in large sizes that are meters long and centimeters in diameter containing multiple atmospheres of $^3$He, and their sensitivity is high enough to detect individual neutrons. Glass fiber detectors [27] that are doped with $^6$Li can also be made in large sizes, and used for neutron detection where physical ruggedness or flexibility in shape is important. However, the glass-fiber detectors generally have lower intrinsic detection efficiency and less robust gamma-ray discrimination than $^3$He-based instruments.

Typical commercial RPMs use multiple polyethylene-moderated $^3$He tubes. Although the different RPM vendors utilize slightly different algorithms, their thresholds for neutrons are usually based upon a multiplier of a background count-rate distribution width, and account in some way for the statistics of small numbers. A typical method is to calculate the dynamic thresholds ($T$) from the background counts ($B$) in a certain time interval and a variable multiplier ($m$) that is determined by a calibration process. The signal is usually accumulated as a running sum over some time period and compared to this dynamic threshold as determined from the background preceding vehicle occupancy of the portal. The smaller the value of $m$ is, the greater the sensitivity of the system, and the higher

the potential false alarm rate resulting from noise or statistical variations. One typical implementation of a dynamic threshold $T$ based on a pre-occupancy background counts of $B$ would be

$$T = B + m\sqrt{B} + c.$$

The constant $c$ in this equation is a small number (typically between 1 and 2) to handle the situation of fluctuations in the small background values that could result in $B$ being zero. The sigma multiplier $m$ allows the threshold to be varied and the neutron detector threshold to be set as low as possible while minimizing false alarms due to statistical fluctuations. Note that the relationship given above assumes that $B$ can be described by a Gaussian distribution, which is not always the case in low-count-rate neutron detection. Relationships based on Poisson statistics, however, are similar in concept. A recent paper by Blessinger et al. [28] discusses possible alternative algorithms for neutron detection.

The $^3$He proportional counters typically used for neutron detection in RPM systems are sensitive to acoustic noise and radiofrequency interference. Thus, the counters and electronics for these detectors need to be designed and installed to have adequate radiofrequency shielding and to have vibration and shock isolation. Requirements for these environmental factors are included in the American National Standards Institute (ANSI) standards used to test systems for adequate performance for border monitoring applications [29].

Because the cosmic-ray-induced neutron background count rate is very stable at a given altitude, generally varying appreciably only with altitude, an alarm threshold can be set relatively low compared to gross-counting gamma-ray thresholds. And, neutron false alarm rates are generally consistent with predictions based on statistical counting noise alone, which is not the case for gamma-ray sensors. Once thresholds are set, functional testing of the neutron detection system of an RPM must be performed with a known neutron source to verify its correct response.

## 4. Neutron backgrounds

Sources of background radiation include cosmic sources, cosmic-produced secondary radiation, terrestrial sources, and man-made sources. Cosmic sources can vary with the solar cycle and solar activity such as solar flares. The measured cosmic background at the surface of the Earth is influenced by latitude, barometric pressure (including altitude), solar activity, diurnal cycle, and weather. Terrestrial background sources can vary spatially due to the minerals in the soil and temporally by changes in the weather. The vast majority of background neutrons come from cosmic rays, since the distribution of natural uranium in the soil is typically too low to produce many neutrons.[1]

Cosmic radiation incident upon the upper atmosphere primarily consists of charged particles with energies typically above 300 MeV. Primary cosmic particles are about 90% protons, but other charged particles with masses up to iron nuclei are common with traces of heavier element nuclei, possibly including uranium [31]. Upon arrival at the Earth's atmosphere, the primary cosmic radiation particles undergo nuclear interactions through collisions with atmospheric nuclei to produce secondary particles, including neutrons. The number of secondary particles reaching the surface of the Earth is a function of five parameters: latitude, weather, solar activity, time of day, and barometric pressure (including altitude effects). Since primary cosmic particles interact with the atmosphere, longer paths through the atmosphere reduce the flux reaching the ground, resulting in lower background radiation levels. Cosmic radiation is thus highly dependent on elevation with higher backgrounds at higher elevations. Some cosmic radiation-induced secondary neutrons make it to the surface of the Earth, while others are produced at the surface. The flux of background neutrons at the surface of the Earth is dependent upon atmospheric pressure, since pressure directly affects the interaction length for cosmic particles reaching the surface. The energy distribution of this flux near the surface shows a broad maximum around 1 MeV [32–34].

Many researchers have measured the neutron flux near sea level, and they report a range of values. Yamashita et al. [35] report a value of about 72 neutrons/(s m$^2$) near the surface from calculations and 40 neutrons/(s m$^2$) from measurements. Lindstrom et al. [36] report the fast neutron background arising from cosmic rays at sea level is about 200 neutrons/(s m$^2$). Sheu et al. [33] report a total flux at sea level of about 51 neutrons/(s m$^2$) and 29 neutrons/(s m$^2$) near the surface of water. O'Brien et al. [37] report about 64 neutrons/(s m$^2$) near the air–ground interface, 31 neutrons/(s m$^2$) near the surface of water, 210 neutrons/(s m$^2$) near an air–aluminum interface, and 770 neutrons/(s m$^2$) near an air–iron interface. Gordon et al. [38] report about 134 neutrons/(s m$^2$) at Yorktown Heights (altitude of 167 m), which results in about 120 neutrons/(s m$^2$) at sea level, while Goldhagen et al. [39] gives about 122 neutrons/(s m$^2$), and Wiegel et al. [34] state about 125 neutrons/(s m$^2$). The differences in these values may be explained because the measurements were made in different locations and with different instruments. A value of about 100 neutrons/(s m$^2$) appears to be a reasonable average value to assume at sea level.

The neutron background seen in RPMs is a fairly constant low rate of events with occasional short-duration (fraction of a second) spikes. These spikes are attributed to the "ship effect" due to cosmic ray interactions in the surrounding vehicles and environment, as discussed below.

[1]Natural uranium and thorium in soil at the few part-per-million level generate about 0.04 neutrons/(s m$^2$) coming from the surface due to alpha-induced reactions, with a few percent contribution from fission, as measured in Gran Sasso [30].

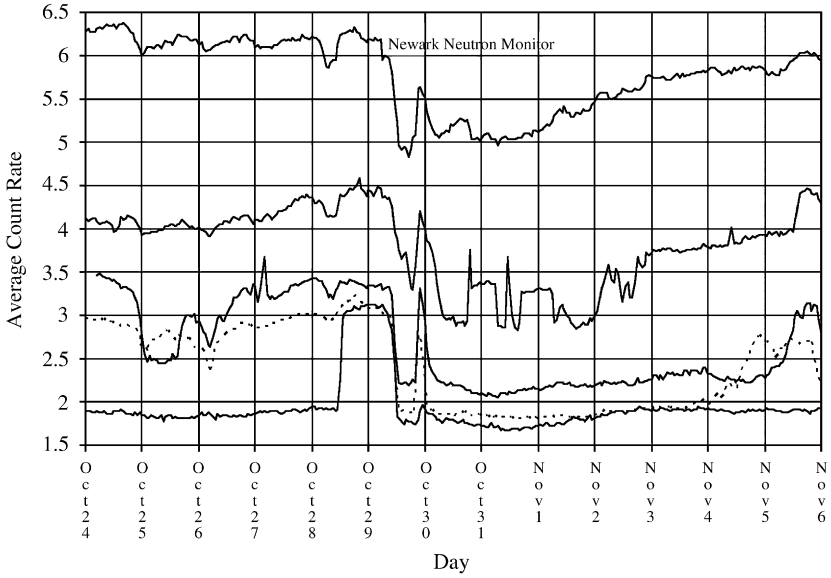


Fig. 2. The neutron count rate measured at the Newark Neutron Monitor in Newark, Delaware (top solid trace) with the neutron count rate measured at four RPM locations shown as the lower four traces. This graph shows hourly counts covering the time period around the large solar flare and following the Forbush decrease that occurred in late October 2003.

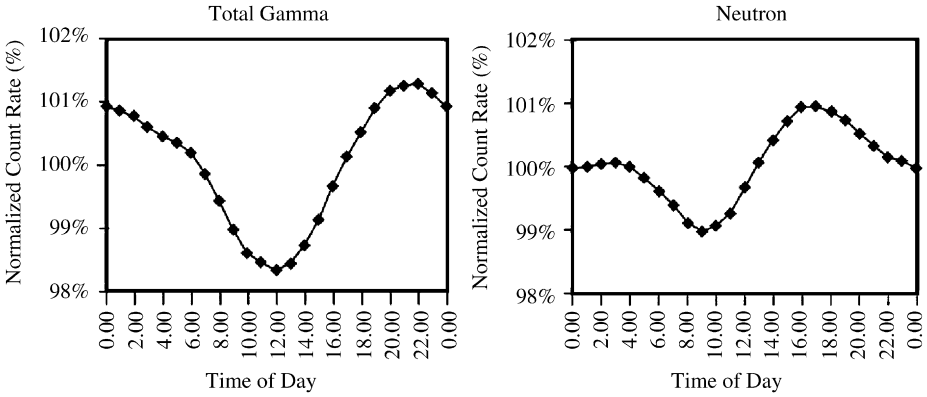


Fig. 3. Average diurnal response of total gamma-ray background and neutron background as a function of time of day. These curves are averaged over all panels, locations, and days.

Many neutron observatories worldwide archive neutron counts at a rate of seconds to minutes [40]. These observatories often provide the uncorrected rates, the atmospheric pressure, and the pressure-corrected count rates. Correlations between observations at these observatories and RPM neutron background rates have been evaluated by the authors.

A large solar event occurred on October 29, 2003, resulting in a 22% decrease in the neutron background count rate at the surface of the Earth. Fig. 2 shows this 13-day event as seen by four, RPM neutron detectors along the northern border of the US and at the Newark Neutron Monitor.[2] It is seen that the average RPM neutron background rate is in the range of a few counts per second. The figure clearly shows that the decrease in cosmic ray background following a flare (Forbush decrease) [41] is visible in the cosmic ray observatory data and also in the measured neutron background at all four RPM locations. The RPM traces tend to track the other features of the Newark monitoring station data. The lowest trace is seen to be from a site with a low background where the statistical variation between two to three counts due to weather condition changes is apparent.

Fig. 3 illustrates that there is a diurnal background variation as observed in deployed RPMs, and that a smaller diurnal relationship exists for neutron background (plot on right) when compared to the gamma-ray background (plot on left). There is a consistent pattern of lower neutron counts in the morning around 09:00 and higher counts in the late afternoon to evening between 16:00 and 18:00. For certain locations in the early morning, there is a minor dip around 02:00 and a minor peak around 03:00. A diurnal fluctuation in cosmic-ray intensity has been well

[2]This neutron monitor was developed for the International Quiet Sun Years (IQSY) of 1964–65 [40].

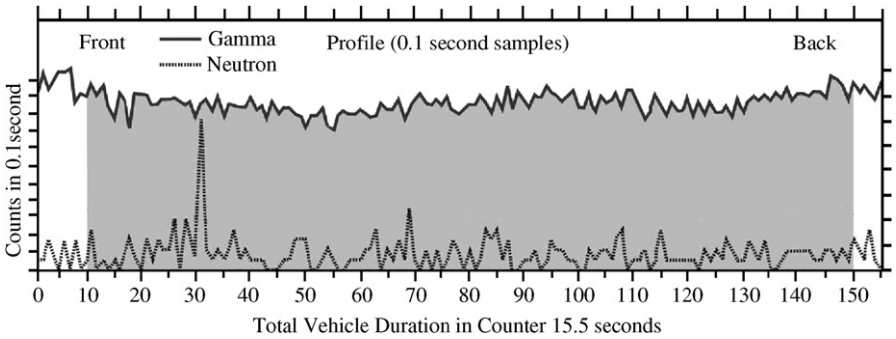


Fig. 4. Neutron spike event (lower trace) induced in an RPM $^3$He-based neutron detector by a cosmic ray event as seen at channel 31. Shown in the upper trace is the gamma-ray count rate that has no indication of any associated event. The neutron and gamma-ray count rates differ by about three orders of magnitude. The time axis is in units of 0.1 s.

known for at least 50 years [42]. This fluctuation is from charged particles in the ionosphere interacting with charged cosmic particles. As solar radiation warms the ionosphere, it becomes more ionized and changes occur in the way it interacts with cosmic particles. Analysis also shows a strong negative correlation between neutron background and barometric pressure, as expected. Most RPM locations showed little relationship between neutron background and season except for a few that were observed by the authors to show a drop in the late autumn and early winter.

## 5. Nuisance/false alarm rates and "ship effect" neutrons

False alarms are produced by RPMs when statistical fluctuations in the background exceed some alarm criterion, from electronic or acoustic noise, or when instruments fail, such as an electrical breakdown. Nuisance alarms are those produced by real radiation sources that are not considered to be a threat. False alarms are exceedingly rare for either neutron or gamma-ray detectors used in RPMs at typical threshold settings. While nuisance gamma-ray alarms are infrequent, they are still significant for RPM gamma-ray detectors, with a frequency of about one in 100 vehicles due to gamma-emitting NORM. On the other hand, neutron nuisance alarms for RPM detectors are rare, with a frequency of about one in 10 000 vehicles at typical operating thresholds. The considerations involved in calculating neutron alarm thresholds for RPMs are different than those for gamma-ray thresholds due to the low ambient neutron background and the infrequency of neutron sources in commerce.

Nuisance neutron alarms arise from commercial sources such as occasional legitimate shipments of nuclear reactor fuel or moisture gauges that contain neutron sources. Nuisance neutron alarms can also arise from occasionally large, short-duration spikes in neutron production from cosmic rays interacting in nearby material, such as cargo. If a large amount of metal in a typical 40-ft inter-modal cargo container (maximum capacity of about 30 t) is scanned by an RPM, the average neutron rate can rise to an observable threshold level above background. These cosmic ray induced neutrons, or "ship effect" neutrons, may be observed around tens of tons of material, especially high atomic weight metals such as lead.

The term "ship effect" arose in the 1970s when neutron detectors were used to look for the presence of nuclear weapons on ships at sea. It was observed that an elevated neutron count rate was present near any large ship, and this was attributed to cosmic-ray-produced neutrons in the iron of the ships. Measurements have shown that the neutron flux near an air–steel interface can be 25 times that at an air–water interface [37]. While there are many articles about cosmic ray related neutrons (see for example Refs. [43–45]), and increased neutrons near the interface between air and other materials [33,35,46,47], there are few open publications about the ship effect. Measurements of ship effect neutrons from 225 to 340 kg (500–750 pounds) of lead that had provided false readings for Pu waste containers were reported by Haggard et al. [48]. A recent article by Kiess [49] references work by Goldhagen [39] that reports on unpublished work measuring ship effect neutron rates aboard cargo container ships. The observed ship effect neutron rates depend on factors mentioned above such as latitude, altitude, weather, and solar activity.

As an example of the size of the ship effect based on extrapolation of previous measurements, at the latitude (46°N) and altitude (136 m above sea level) of Pacific Northwest National Laboratory (PNNL), a shipping container filled with about 10 t of Celotex (building material consisting of low atomic weight elements) can emit about 80 neutrons/s; a shipping container filled with about 10 t of iron can emit about 200 neutrons/s; and a shipping container filled with about 10 t of lead can emit about 600 neutrons/s.[3] If the amount of material is not so massive, these neutrons may be observed as spikes with very short duration in a neutron detector. These spikes in neutron activity are very different from the continuous signal resulting from real sources in commerce. Under this condition, filtering methods can be used to eliminate most

[3]Richard Arthur (PNNL), private communication, January 2007.

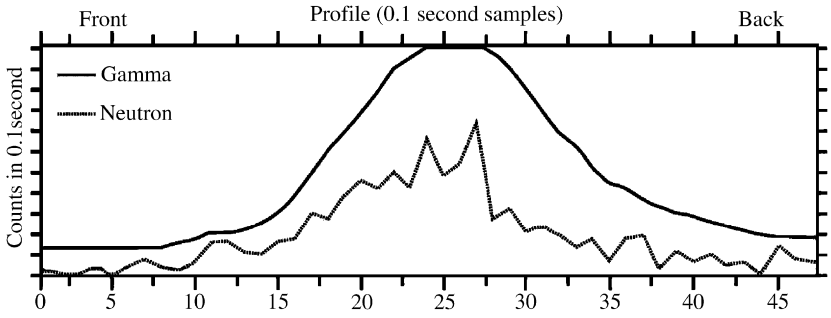


Fig. 5. RPM response to a moving vehicle containing a large distributed neutron and gamma-ray source. The jagged curve is the neutron response. The scales for the neutron and gamma-ray signals are different and arbitrary. The time axis is in units of 0.1 s. The neutron and gamma-ray detectors show a similar distribution in time as the vehicle moves past.

of them. Fig. 4 shows such a spike event observed by the authors in an RPM (around channel 31 in the lower trace).

Unlike the gamma-ray detection threshold, the main considerations in calculating a neutron alarm threshold is the false alarm rate due to statistical fluctuations in the background, and the competing need to have a high probability to detect a minimum target quantity. Because of the lack of significant NORM sources of neutrons, the guiding principle for setting a neutron alarm threshold is to provide the highest sensitivity possible consistent with minimizing the impact of statistical false alarms on operations.

Neutron nuisance alarms are more common for cargo transported across the northern border than on the southern border due to differences in commerce. Nuisance alarms are even less frequent for personally owned vehicles for either border, as would be expected since they would not normally carry commercial sources and their smaller size reduces the chance for ship effect neutrons. As discussed above, neutron-emitting sources include well logging probes, concrete dryness detectors, nuclear fuel, and uranium compounds such as yellowcake. Although the neutrons emitted from these sources can be relatively energetic and penetrate many materials, their enclosures and surrounding cargo will reduce the energy and the flux of the neutrons through scattering and absorption. Energy moderation may make the detection of these neutrons somewhat easier since the neutron detectors used in RPMs are more sensitive to low-energy neutrons, but if too many neutrons are absorbed, detection of the source may not be possible.

Fig. 5 shows the response of an RPM to a vehicle with both large, distributed neutron and gamma-ray sources. The trace shows a broad feature, rather than a narrow spike in time as would be produced by a spallation event (Fig. 4), which is characteristic of a distributed neutron source being moved past the detector. A point neutron source would also show a somewhat broad distribution due to the poor spatial resolution of the neutron detector, but to a lesser extent. All such sustained neutron signals are investigated thoroughly since they indicate a non-cosmic source that may be of concern.

## 6. Threat detection

The intent of a nuclear interdiction technology system is to detect the presence of threat items, which for the case of neutron detection technology means the possibility of detecting plutonium or HEU, either as material or in a weapon of mass destruction or improvised nuclear devices. The fact that a mass of 4 kg of plutonium, or 25 kg of HEU, is sufficient for a nuclear explosive device is unclassified, and thus these masses are used for the calculations presented in this paper. These values are similar to the "significant quantities" of 8 kg of plutonium and 25 kg of HEU utilized by the International Atomic Energy Agency for safeguards applications [18]. Smaller quantities would generally be more difficult to detect than these amounts, so these quantities may be considered as optimistic sources from a detection point of view.

If delta phase plutonium metal (density of $15.92 \times 10^3$ kg/m$^3$ [50]) were in the form of a solid sphere, 4 kg of plutonium would have a radius of about 39 mm. If HEU metal (density of $19.07 \times 10^3$ kg/m$^3$ [50]) were in the form of a solid sphere, 25 kg of HEU would have a radius of about 68 mm. Weapons grade plutonium (WGPu) can have a variety of assumed compositions. For simplicity, it will be assumed here that WGPu is initially composed of only 90% $^{239}$Pu and 10% $^{240}$Pu, without the small amounts of minor isotopes that are usually present, and is 1 year old. Similarly, HEU is assumed here to be initially composed of only 90% $^{235}$U and 10% $^{238}$U, without any minor isotopes present, and is 1 year old. These minor isotopes, when present, tend to increase the neutron and gamma-ray signature of these materials (by factors of two or more). DU is assumed here to be 0.2% $^{235}$U and 99.8% $^{238}$U.

Emission rate distributions for both neutrons and gamma rays were calculated using configurations as listed in Table 1. The calculations were performed in two steps: (1) spectral distributions for 1-g amounts of source material were produced, and (2) these "elemental" spectral distributions were used as input for Monte Carlo N-Particle (MCNP) calculations [51] of spectra emitted from the surface of multi-kg-sized, solid metallic spheres of the sources shown in Table 1.

Table 1
Properties of weapons grade plutonium (WGPu), highly enriched uranium (HEU), and depleted uranium (DU) used in this study

| Source | WGPu | HEU | DU |
|---|---|---|---|
| Composition, mass% | 90.0 $^{239}$Pu<br>10.0 $^{240}$Pu | 90.0 $^{235}$U<br>10.0 $^{238}$U | 0.2 $^{235}$U<br>99.8 $^{238}$U |
| Mass, kg | 4 | 25 | 25 |
| Density, $10^3$ kg/m$^3$[a] | 15.92 | 19.07 | 19.07 |
| Sphere radius, mm | 39.1 | 67.9 | 67.9 |
| Neutron production per gram, neutrons/(s g)[b] | 130 | 0.00136 | 0.0135 |
| Neutron multiplication[c] | 2.14 | 2.84 | 1.05 |
| Total neutrons from sphere, neutrons/s[c] | $1.11 \times 10^6$ | 97 | 355 |
| Emitted decay photons, photons/(s g)[d] | $1.85 \times 10^8$ | $1.51 \times 10^5$ | $3.93 \times 10^3$ |
| Photon multiplication[e] | $5.82 \times 10^{-5}$ | $2.44 \times 10^{-3}$ | $4.26 \times 10^{-3}$ |
| Neutron induced photons from sphere, photons/s[e] | $3.11 \times 10^5$ | 22.1 | 20.4 |
| Decay photons from sphere, photons/s[e] | $4.31 \times 10^7$ | $9.22 \times 10^6$ | $4.19 \times 10^5$ |
| Bremsstrahlung photons from sphere, photons/s[e] | – | $5.14 \times 10^4$ | $5.20 \times 10^5$ |
| Total photons from sphere, photons/s[e] | $4.34 \times 10^7$ | $9.27 \times 10^6$ | $9.39 \times 10^5$ |

[a]See Ref. [5].
[b]LANL SOURCES-4A computational result [60].
[c]MCNP computational result [43].
[d]SYNTH computational results for decay photons of all energies [56].
[e]MCNP computational result summed for $E > 30$ keV [43].

For the first step, the code SOURCES-4A [52] was used for the 1-g fission neutron distributions, and the code SYNTH [53] was used for the 1-g decay gamma distributions by aging the initial isotopic blends by one year. These source values from [52] were found to be slightly higher (~25%) for WGPu than found in [54], while they agreed for HEU.

Because $^{234m}$Pa and $^{234}$Th are in secular equilibrium with the decay of $^{238}$U, and because they are beta emitters, MCNP was used to obtain their corresponding 1-g Bremsstrahlung gamma-ray distributions for the $^{238}$U components of the sources studied. Only the Bremsstrahlung contribution from $^{234m}$Pa was significant, however, because its beta spectral distribution extended beyond 2 MeV. The beta spectrum of $^{234}$Th did not extend beyond 175 keV, and its Bremsstrahlung contribution was two-orders of magnitude smaller than that for $^{234m}$Pa.

Neutrons are produced by spontaneous fission, plus there is a multiplication effect in the sphere of metal from induced fission. Table 1 shows the spontaneous fission neutron rate emitted per gram of source material, times the mass and the multiplication factor (which was derived from MCNP results), gives the total emission rate from the spheres.

For comparison purposes, it is useful to understand the origin of the gamma-ray flux from the same sources. Gamma rays are produced by photon emission following spontaneous fission, by neutron-induced photons, and by Bremsstrahlung photons following beta decay. All of these components are included in the results shown in Table 1. The photon emission rate from the decay per gram of isotope includes all photons, while the photon emission rates from the spheres are the sum of all photons above 30 keV. The self-attenuation effect of the spheres, parameterized as the photon multiplication, is seen to be large due to the loss of most low-energy photons inside the sphere. This is a larger effect for WGPu than HEU because WGPu has intense low-energy gamma rays below 30 keV.

The evaluations described above give the spontaneous fission neutron emission rate from $^{239}$Pu to be only about 0.03 neutrons/(s g) and from $^{240}$Pu to be about 1300 neutrons/(s g) [52]. These values can be used for small masses, but for large masses, self-attenuation and multiplication in a specific geometry need to be taken into account. Assuming no multiplication, a 4-kg WGPu sphere would emit about $0.52 \times 10^6$ neutrons/s. With multiplication, it was found that about $1.11 \times 10^6$ neutrons/s were emitted from a 4-kg metallic sphere of WGPu.

The spontaneous fission neutron emission rate from $^{238}$U is about 0.0136 neutrons/(s g) and from $^{235}$U is about $3 \times 10^{-4}$ neutrons/(s g) [54]. Assuming no multiplication of neutrons, a 25-kg metallic HEU sphere would emit about 34 neutrons/s, while about 97 neutrons/s was found with multiplication. For comparison, a metallic sphere made from 25 kg of DU would emit about 338 neutrons/s, without multiplication [54], and with multiplication, it was found to be about 355neutrons/s.

From these computed values that are benchmarked against the literature mentioned above, it is apparent that HEU emits about four orders of magnitude fewer neutrons than WGPu for these specified quantities and composition and is thus a challenge to detect via neutrons. For example, a one square meter neutron detector with a realistic

intrinsic detection efficiency[4] of 10% at a distance of 2 m (about 2% solid angle) would detect only about 0.2 neutrons/s from the HEU mass, while detecting 2200 neutrons/s from the WGPu mass.

For these same masses of WGPu (4 kg), HEU (25 kg), and DU (25 kg), there would be $43.4 \times 10^6$, $9.3 \times 10^6$, and $0.94 \times 10^6$ photons per second, respectively, emitted above 30 keV including self-attenuation effects. In the absence of substantial shielding, this gamma-ray signature is thus far easier to detect than the neutron signal, especially from HEU. If there was significant gamma-ray shielding, but not specific neutron shielding, the WGPu neutron signal is substantial, but that from HEU is very difficult to observe.

## 7. Simulation of neutron sources

Modeling and simulation play a central role in determining the characteristics of radiation transport and detection systems for national security applications. We have applied the MCNP radiation transport code for investigation of the neutron sources, neutron and gamma-ray transport, and detector simulation [51]. This and the next sections consider some results from the simulations of sources and detectors.

A model was constructed of a $^{252}$Cf source surrounded by various cargos in the center of a cubic inter-modal cargo container (IMCC) that is 2.44 m (8 ft) on a side. The cargo was assumed to surround the source in spherical shells and the neutron flux coming out of one side of the container was tallied. Four thicknesses of spherical shells were used, constructed from five concentric spherical surfaces with radii 25 mm, 0.275 m, 0.525 m, 0.775 m, and 1.025 m. The volume inside the smallest sphere surrounding the source was filled with air, and the remaining four shells defined the 0.25-m radial increments of cargo amounts studied. Simulations of kitty litter (an absorbent bentonite clay product), fertilizer, polyethylene, pine, and iron cargo were computed in order to show the down scattering and absorption of the neutrons through various cargo thicknesses. To cover the energy range from 1 eV to 10 MeV, the energy bins in the MCNP calculations were chosen to be equally spaced logarithmically.

Figs. 6–10 show the percent emission efficiency (neutrons emerging per source neutron emitted) per keV from one wall of the IMCC as a function of energy for a $^{252}$Cf neutron source surrounded by varying thicknesses of the different materials—kitty litter, fertilizer, polyethylene, and iron, respectively. None of these results for any of the cargos include ship-effect neutrons. These figures present the data as lethargy plots. These plots demonstrate the clear effects on the initial fission neutron spectrum of the various cargos.

Since these plots show the spectra only down to 1 keV, Table 2 gives the percent of emitted neutrons from these

[4]The intrinsic detection efficiency is the ratio of detected neutrons compared to the number impinging on the detector.

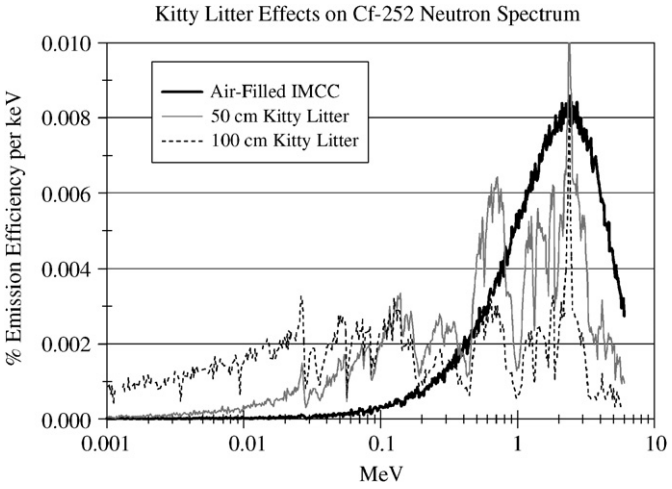


Fig. 6. Lethargy plot of percent emission efficiency as a function of energy of a $^{252}$Cf neutron source surrounded by varying thicknesses of dry kitty litter.

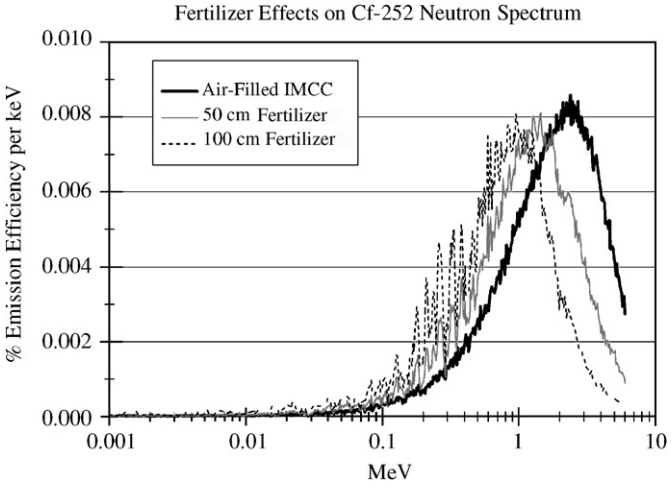


Fig. 7. Lethargy plot of percent emission efficiency as a function of energy of a $^{252}$Cf neutron source surrounded by varying thicknesses of fertilizer.

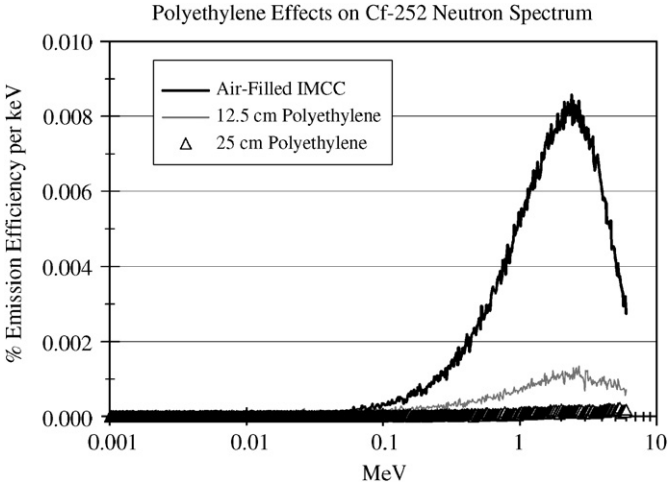


Fig. 8. Lethargy plot of percent emission efficiency as a function of energy of a $^{252}$Cf neutron source surrounded by varying thicknesses of polyethylene.

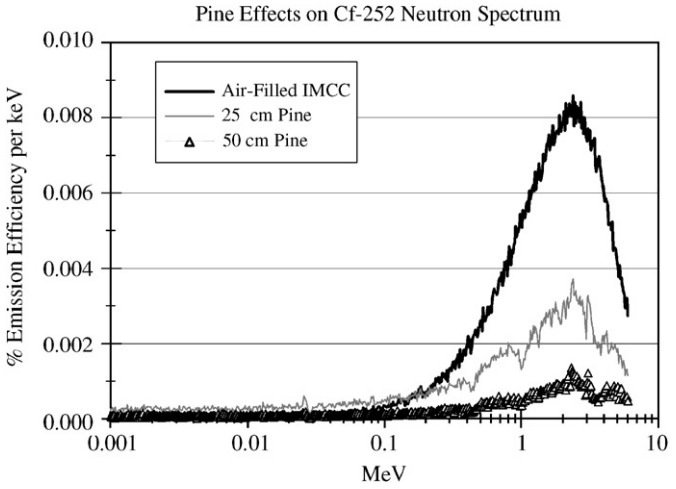


Fig. 9. Lethargy plot of percent emission efficiency as a function of energy of a $^{252}$Cf neutron source surrounded by varying thicknesses of pine.

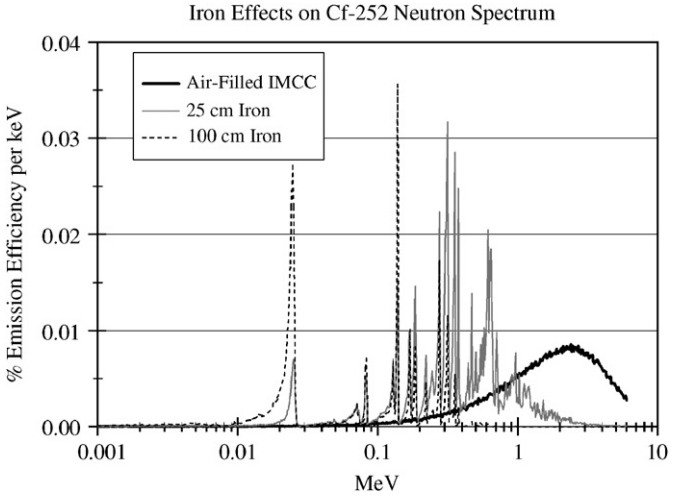


Fig. 10. Lethargy plot of percent emission efficiency as a function of energy of a $^{252}$Cf neutron source surrounded by varying thicknesses of iron (density = $7.86 \times 10^3$ kg/m$^3$).

Table 2
Percent of emitted neutrons below 1 keV, and "full-energy" percent emission efficiency (neutrons through one surface) for a $^{252}$Cf source in various cargo shielding conditions

| | Percent below 1 eV | Percent below 1 keV | Percent emission efficiency |
|---|---|---|---|
| No cargo in container | 0.1 | 0.1 | 98 |
| Kitty litter (cm) | | | |
| 25 | 0.02 | 0.2 | 98 |
| 50 | 0.05 | 0.7 | 99 |
| 75 | 0.2 | 3.5 | 99 |
| 100 | 0.8 | 12 | 98 |
| Fertilizer (cm) | | | |
| 25 | 0.02 | 0.2 | 97 |
| 50 | 0.02 | 0.2 | 95 |
| 75 | 0.02 | 0.3 | 93 |
| 100 | 0.02 | 0.3 | 92 |
| Polyethylene (cm) | | | |
| 12.5 | 47 | 55 | 40 |
| 25 | 51 | 58 | 5.3 |
| 50 | 40 | 48 | 0.1 |
| 75 | 21 | 21 | 0.01 |
| 100 | 100 | 100 | 0.0003 |
| Pine (cm) | | | |
| 25 | 31 | 43 | 85 |
| 50 | 56 | 64 | 39 |
| 75 | 62 | 68 | 13 |
| 100 | 62 | 67 | 4 |
| Iron (cm) | | | |
| 25 | 0.06 | 0.8 | 99 |
| 50 | 0.1 | 1.7 | 92 |
| 75 | 0.2 | 3.1 | 75 |
| 100 | 0.2 | 4.4 | 53 |

various cargo scenarios below 1 keV and below 1 eV. This shows the strong moderating effect of pine and polyethylene. These two materials thermalize about half of the neutrons that survive and escape the material, which strongly impacts their detection by a moderated neutron detector. The table also provides the percent emission efficiency for each scenario; this value is normalized to 100% if no neutrons were absorbed in the cargo. The table shows that kitty litter, fertilizer, and to a large degree, iron, do not absorb many neutrons, while polyethylene and pine strongly impact the number of neutrons escaping the cargo container. Table 3 provides information on the composition and density used in the simulations for each of these cargo materials.

From Fig. 6 it can be seen that kitty litter moderates a sizable fraction of the neutrons, distorts the neutron energy spectrum, and absorbs some of the neutrons. The impact of this moderation of the neutron spectrum from a fission source on the detection of these neutrons will be discussed later. The kitty litter simulated in this work has only a weak gamma-ray emission rate from the uranium and thorium decay chains and $^{40}$K.

Fig. 7 shows that fertilizer somewhat moderates the neutrons, distorting the energy spectrum, but absorbing few of them. The fertilizer modeled in this work has a strong gamma-ray emission rate from its $^{40}$K content, while other fertilizer types may also contain uranium and thorium chains as well.

In contrast to kitty litter and fertilizer, polyethylene (Fig. 8) has a major impact on the neutron flux, eliminating most of them with a thickness of about 0.25 m. This strong attenuation of the neutron flux by polyethylene is accompanied by an increase in the gamma-ray flux produced by the neutron capture reaction. In order to shield a neutron emitting threat, an engineered shield for both the neutrons and secondary gamma rays would be required, and would be physically large in diameter. Polyethylene is not otherwise an emitter of a significant number of gamma rays.

Table 3
Detection efficiency for a $^{252}$Cf source in various cargo shielding conditions

| Cargo type | Atomic fraction | Density (g/cm$^3$) | Relative detection efficiency | | |
|---|---|---|---|---|---|
| | | | Cargo thickness | | |
| | | | 100 cm | 50 cm | 25 cm |
| Kitty litter | 0.615 O<br>0.077 Al<br>0.231 Si<br>0.077 K | 0.87 | 0.971 | 1.048 | – |
| Fertilizer | 0.002 H<br>0.002 O<br>0.014 Na<br>0.498 Cl<br>0.484 K | 1.0 | 1.047 | 1.050 | – |
| Polyethylene | 0.666 H<br>0.333 C | 0.93 | – | 0.018 | 0.195 |
| Pine | 0.486 H<br>0.286 C<br>0.238 O | 0.5 | – | 0.197 | 0.625 |
| Iron | 1.0 Fe | 7.9 | 0.479 | – | 1.091 |

Values are relative to a detection efficiency of 1 with no intermodal cargo container (IMCC) or cargo. The detection efficiency for an empty IMCC is 1.027. Dashes indicate that values were not computed.

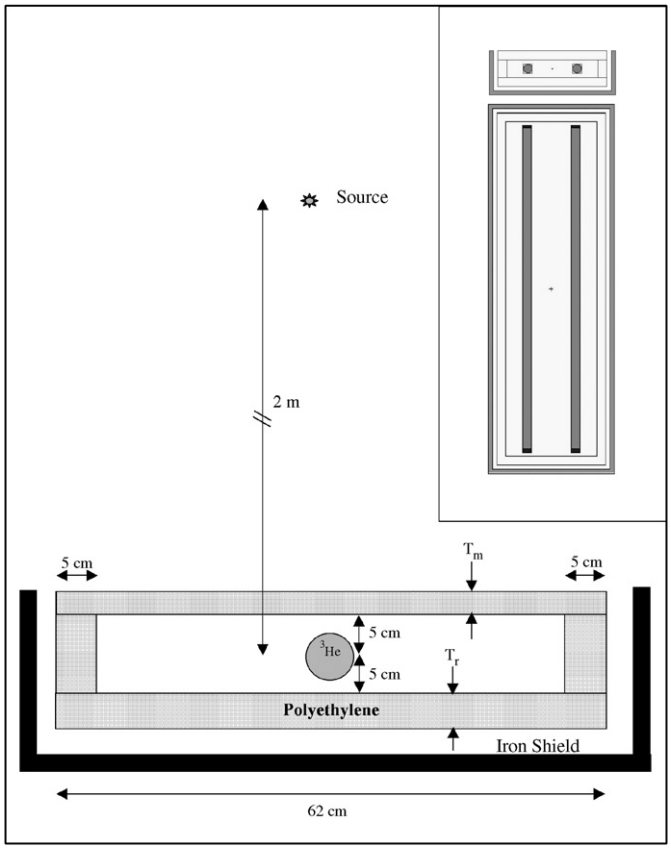


Fig. 11. Cross-sectional view of the neutron detector geometry used for the MCNP calculations with a neutron source located 2 m from $^3$He neutron detector inside a polyethylene box with variable front and back wall thicknesses. The inset shows a vertical and horizontal cross-section of the assembly with two tubes.

In Fig. 9, it can be seen that the pine also has a significant impact on the emission efficiency, absorbing the neutrons, but not as dramatically as polyethylene. This attenuation of the neutron flux is accompanied by an increase in the gamma-ray flux produced by the neutron capture reaction. Pine is otherwise not an emitter of a significant numbers of gamma rays.

Iron (Fig. 10) can be seen to have resonances that selectively capture certain bands of neutron energies, but that overall absorption is relatively low compared to hydrogenous materials. Iron is not a significant emitter of gamma rays.

## 8. Simulation of neutron detection

To show some of the effects on neutron detection from changes in detector geometry, a series of MCNP calculations were performed using a model of an $^3$He-type neutron detector characteristic of those commonly used in RPMs. The model of the physical detector is shown schematically in Fig. 11, while the results of these calculations are shown in Figs. 12–15.

The detector geometry, as viewed end-on in cross-section in Fig. 11, is one or two $^3$He neutron tubes, with an active length of 1.83 m (72 in.), a pressure of 300 kPa (3 atm) at 0° C, a variable thickness ($T_m$) polyethylene moderator in front, and a variable thickness ($T_r$) polyethylene reflector in back. The center of the 49.9-mm (1.96-in.) internal-diameter $^3$He tube is fixed at 50 mm from the inner reflector and moderator surfaces. The sides and ends of the assembly are capped with 50 mm of polyethylene, forming a complete enclosure for the $^3$He tube. This gives an external dimension for the polyethylene assembly of 0.62 m wide by 2.01 m long. The total thickness of the polyethylene box is thus equal to $0.010\,\text{m} + T_m + T_r$. For some results, as noted below, a 25-mm thick steel enclosure was also included that surrounds five sides of the polyethylene assembly, and is separated from it by 25 mm. A $^{252}$Cf point source at 2.0 m from the center of the neutron tube is used in the model to calculate the detector system response to a fission neutron spectrum. At 2 m from the point source, the fraction of the $4\pi$ solid angle subtended by the active area of the detector tube is $1.7 \times 10^{-3}$, while this fraction is about $2.2 \times 10^{-2}$ for the polyethylene box.

Before discussing the effects of varying the detector geometry, Fig. 12 shows the baseline detection efficiency of an isolated $^3$He tube. The upper plot of Fig. 12 shows cross-sections for the $n + {}^3$He reaction in barns for incident neutron energies up to 10 MeV. The total cross-section drops by over four orders of magnitude across this energy range, and is seen to be dominated by the $^3$He(n,p)$^3$H reaction up to a few keV.

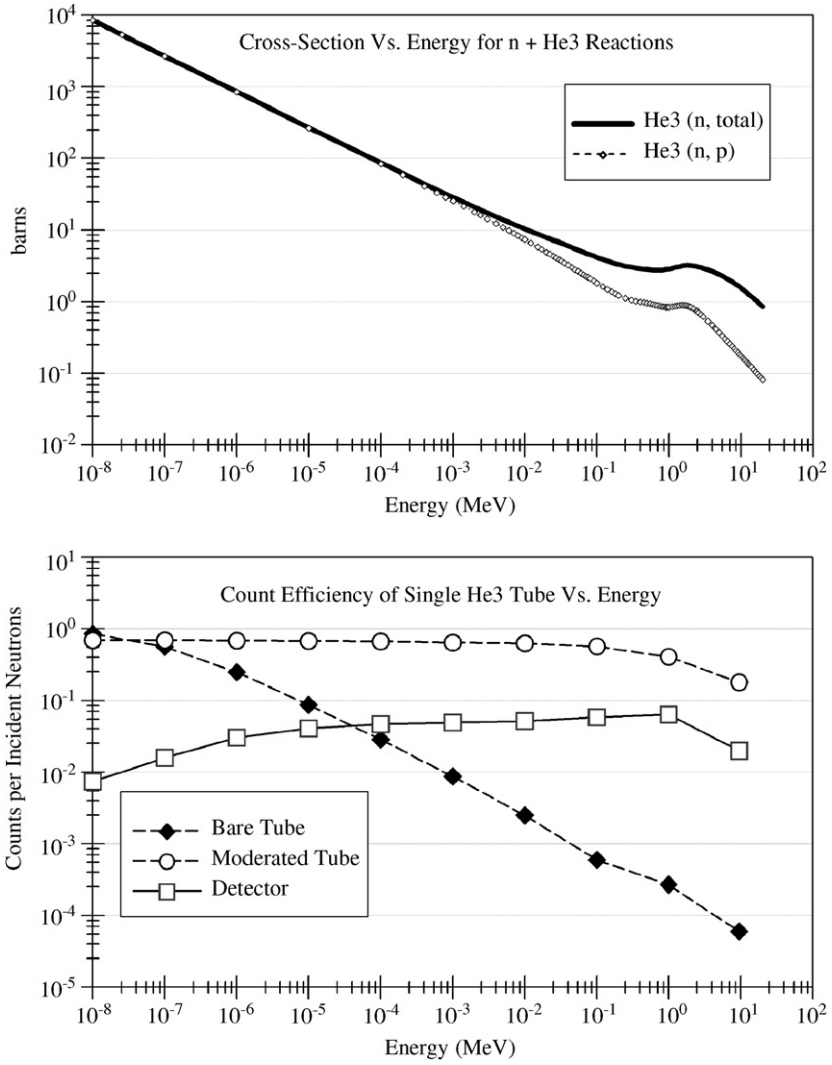


Fig. 12. The upper plot shows the cross-section for the $n + {}^3He$ reaction in barns for incident neutron energies up to about 10 MeV. The lower plot shows three curves: the response of a single unmoderated $^3He$ neutron tube in counts per incident neutron as a function of incident neutron energy, the response of a moderated tube, and the response of a moderated detector assembly. Tick marks on the axes are at 1.5 units.

The curve marked by diamonds in the lower plot of Fig. 12 shows the response of a single, bare unmoderated $^3He$ neutron tube in counts per incident neutron as a function of incident neutron energy up to 10 MeV. This is the ratio of the number of detected neutrons to the number of neutrons impinging on the tube at the same energy (intrinsic efficiency). The response drops by over four orders of magnitude across this energy range. At very low neutron energies, the tube is seen to be almost black (totally absorbing) with respect to the incident neutrons, but is only about 1% efficient for capturing neutrons at 1 keV. This demonstrates the necessity of moderating incident neutrons in order to increase their detection probability.

For the other two curves of the lower plot of Fig. 12, the $^3He$ tube is inside the moderator box described above with 50 mm of polyethylene on all sides. The "moderated tube" curve (open circles) shows the impact of the moderator in increasing and flattening out the detection probability versus emitted neutron energy. This curve is the ratio of the number of neutrons detected (from all sides) to the number originally directed at the tube at the energy shown (intrinsic efficiency). The curve falls slightly below that of the bare tube at the lowest energies due to absorption in the moderator, but remains close to 1 and almost flat out to 1 MeV. This demonstrates the effect of moderating the incident neutrons to increase their detection probability.

The "detector" curve (open squares) of the lower plot of Fig. 12 shows a more important ratio: the number of detected neutrons to the number of neutrons that impinged on the full area (0.62 m wide by 2.01 m long) of the polyethylene moderator facing the source, binned by the initial neutron energy from the source (absolute efficiency). This curve falls one to two orders of magnitude below the "moderated tube" curve simply due to the increased solid angle used in the denominator (a neutron can hit anywhere

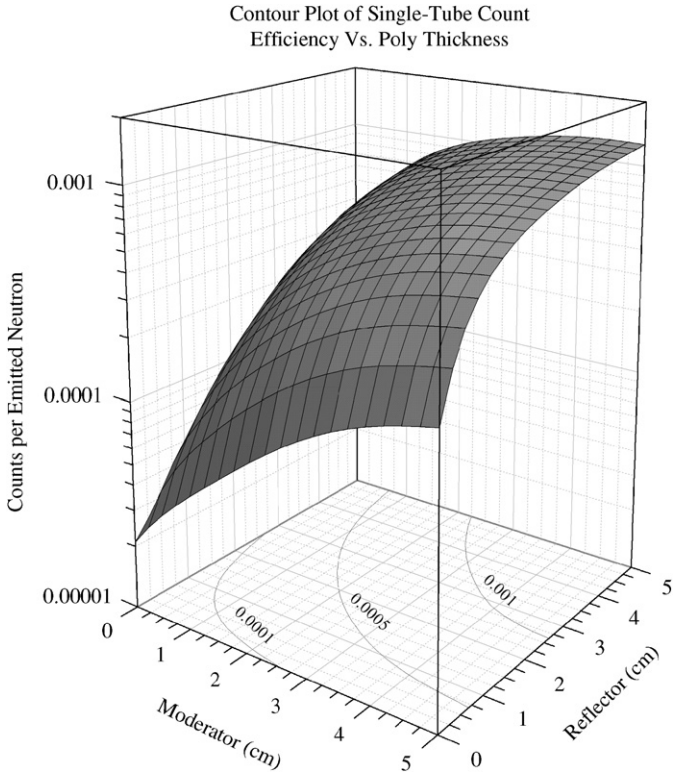


Fig. 13. Efficiency of detection of the source as a function of the moderator and reflector thickness from zero to 50 mm. The vertical axis is the observed counts in the detector assembly per neutron emitted by the source.

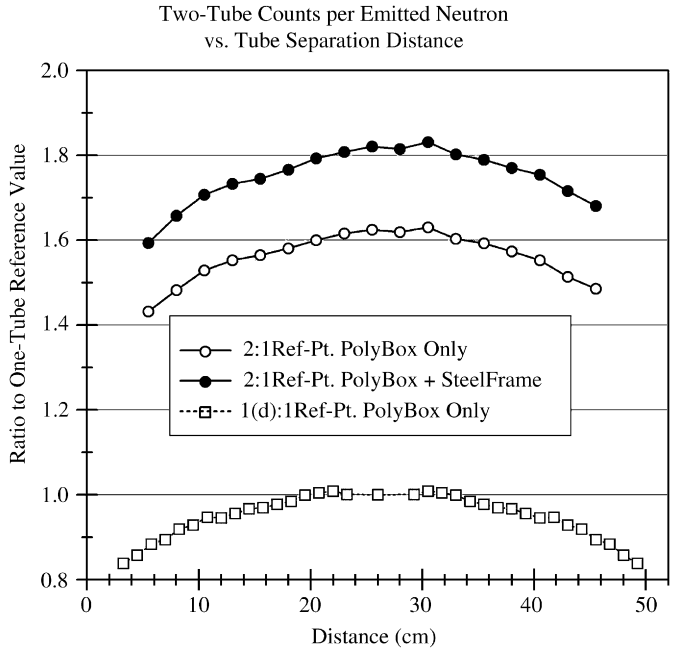


Fig. 14. Efficiency of detection of the source for a one-tube detector assembly as a function of the tube position, and a two-tube detector assembly as a function of the spacing between the two tubes, shown as the ratio to the one-tube maximum efficiency.

on the polyethylene box). The curve then rises somewhat from the lowest energies where neutron absorption is more significant and then falls only at the highest energies above 1 MeV. Note that this curve differs from the "moderated tube" curve by more than just a constant, solid-angle factor (of about 0.08) since the lowest energy neutrons are absorbed in the moderator before reaching the tube. Thus, the moderator design is seen to be fairly optimal for detecting neutrons at all energies of interest.

Fig. 15. Screen capture of MCNP model of the large area neutron detection system consisting of 320 two-tube detector assemblies. The cut-away shows the arrangement of tubes in the assembly. The coordinate vectors shown are 1 m long.

Fig. 13 shows the efficiency for detection of the $^{252}$Cf source neutrons as a function of the moderator and reflector thickness with a single $^{3}$He tube in the geometry described above. The moderator and reflector thickness varied from zero to 50 mm. The vertical axis is the absolute detection efficiency, i.e., detected counts per emitted neutron of all energies. With no polyethylene around the $^{3}$He tube, the efficiency for detecting this source is found to be $4.4 \times 10^{-7}$. Placing a 50 mm polyethylene frame around four sides of the $^{3}$He tube, but with no moderator or reflector, raises the efficiency substantially to $2.1 \times 10^{-5}$ due to the reflection and, very importantly, moderation of neutrons hitting the frame that are scattered into the tube. The figure shows that the efficiency rises monotonically to $1.3 \times 10^{-3}$ as the moderator and reflector thickness are each increased to 50 mm. This efficiency can be compared to the fractional solid angle (out of $4\pi$) of 2.4% as computed for any neutron hitting the front of the 0.62 m by 2.01 m detector assembly, whose face is at 1.90 m from the point source. Thus, about 5.4% of those neutrons hitting the polyethylene detector assembly are actually detected (the intrinsic efficiency). The reflector is seen to have a more dramatic effect on the efficiency than the moderator.

Another series of calculations were performed for the same detector assembly, having 50 mm of polyethylene on all six sides, but with a second $^{3}$He tube inserted. These series of results were obtained with and without including the steel frame. The results are plotted in Fig. 14 as a function of the spacing between the centers of the two tubes. The values are shown as the ratio of the two-tube efficiency to the maximum one-tube efficiency (when the one tube is in the center of the no-steel frame assembly). The two tubes are centered in the box and moved apart with a center-to-center tube distance ranging from 50 mm to 0.45 m.

From Fig. 14, it can be seen that the tubes shadow each other and reduce the effectiveness of each when close together. There is an optimal spacing for this geometry of about 0.30 m where the efficiency is a maximum. The efficiency with two tubes and only the polyethylene box is seen to have a maximum value of over 1.6 times that of the single-tube efficiency, or $2.1 \times 10^{-3}$. The efficiency with two tubes, the polyethylene box, and the steel frame is seen to have a maximum value of over 1.8 times that of the single tube efficiency, or $2.3 \times 10^{-3}$; a 10% improvement over the case where no steel frame is present. Thus, the maximum efficiency for the detection of a neutron that hits the polyethylene box with two tubes is 8.8% with no steel and 9.6% with the steel frame compared to the value of 5.4% for the one tube, no-steel frame assembly given above. Adding a second tube with the proper spacing in this configuration significantly improves the efficiency, but does not quite double it—even with adding the steel frame.

As a reference to the position dependence of a single tube, Fig. 14 also shows the efficiency of detection for the one-tube case when the tube is moved within the polyethylene box from the left edge to the right edge (the center is at 0.26 m on this scale). The efficiency value is shown as the ratio to that obtained at the center, and thus has a maximum value of one in the center. The efficiency is seen to drop by about 16% as the tube is moved away from the center to the edge of the polyethylene box. If the detected flux was coming from neutrons entering only through the front of the $^{3}$He tube (i.e., fractional solid angle subtended by the tube's cross-sectional area of 1.821 m by 50.8 mm), then the decrease in its efficiency by moving it over this same distance would have been 0.6%. This again shows the importance of the polyethylene sides and back of the complete detector assembly.

In order to show the effect of cargo on the detection of a neutron source, the neutron energy spectra from the five cargo scenarios (kitty litter, fertilizer, polyethylene, pine, and iron) discussed in Section 7 of this paper were used. The detector for these models had two $^{3}$He tubes separated by 30 cm with 50 mm of polyethylene on all sides and the steel box. The tubes were located 2 m from the source at the center of the cargo container. Table 3 shows the results from these computations. The values shown in the table are normalized to the value of one for detection of the bare $^{252}$Cf source with no cargo or cargo container. The value shown for the empty IMCC is somewhat larger than one due to reflection of neutrons off the wooden floor of the container into the detector. The table shows that for thicknesses of 25 cm of iron, 50 cm of kitty litter, and fertilizer up to 100 cm, there is an increase in the neutron signal due to moderation of the neutrons in the cargo without substantial absorption. The 100 cm iron cargo only diminishes the neutrons by about a factor of two. The pine and polyethylene on the other hand show very significant absorption of the neutrons even at 25 cm thickness. The conclusion from these simulations is that some cargos may actually enhance the detection of neutrons, while those containing a significant fraction of hydrogen can severely impact the detection of a neutron source. A later report will provide results of experimental comparisons to these modeling results. Previous experimental validation has shown agreement of such detailed simulations to experiment to within about 20%, where the modeling tends to overestimate the response since it does not include some factors, such as electronics, which reduce efficiency.

## 9. Large area detection array for HEU

From the quantitative analysis presented above, it is seen that under comparable shielding conditions, neutron detection of a significant quantity of plutonium is much easier (by about four orders of magnitude) than HEU. Thus, based upon their neutron emissions alone, the typical RPM system is able to detect the presence of significant quantities of plutonium, but not of HEU [4]. Instead, interdiction of HEU typically depends upon gamma-ray detection, even though the largest gamma signal, at 185 keV, is relatively easily shielded. There is a higher-energy gamma signal at 1001 keV from the $^{238}$U in HEU that is more penetrating, but weaker than the 185 keV signal. Plutonium is detectable by both its gamma-ray and neutron emissions.

Although the possibility of detecting the neutron signal from HEU has typically been ignored as impractical, recent concepts for improving upon HEU detection by means of its neutron signal have been made. Gilliam et al. [55] have proposed a neutron coincidence detection scheme for drive-through portals that could potentially detect very large neutron sources, but not small ones. A systems approach has been taken by Wein et al. [56] to the interdiction problem whereby a mathematical model is developed for an optimal inspection strategy to prevent a nuclear weapon (or nuclear material to make a weapon) from being smuggled into the US in a shipping container. In a related paper, Wein et al. [57] argue for an extended series of neutron detectors through which a truck passes, as being a more effective means to detect the neutron signature from a combined HEU and plutonium threat than currently deployed systems.

As suggested by Wein et al. [57], more consideration should be given to detection of neutrons emitted by HEU. Given a large enough detector, and enough measurement

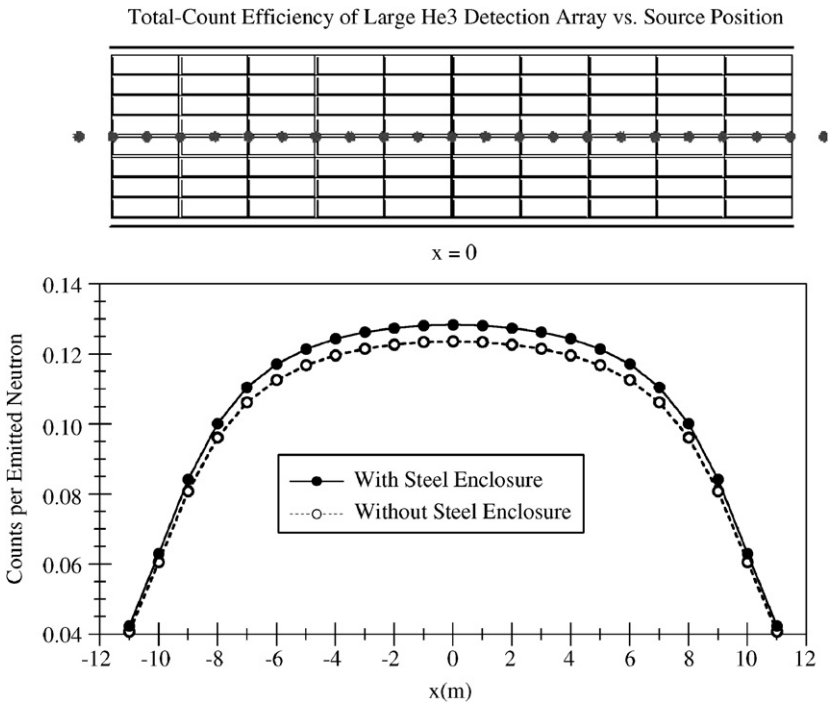


Fig. 16. Response of the large detector array neutron detection system to a neutron source as a function of source position along the length of the detector. The upper schematic shows the individual source positions within the detector assembly. The graph shows the absolute efficiency as a function of this position with and without the steel enclosure around the outside of the detector array.

time, detecting neutrons from HEU in cargo may be feasible for some scenarios. But long measurement times would also potentially create a significant cost and impact on commerce. The following model analysis addresses this question: is it feasible to build a large detection system for the neutrons emitted from a significant quantity (~25 kg) of HEU that would not impede commerce?

Consider a possible neutron detector that is sensitive enough to detect HEU without slowing commerce significantly. This requires measurement times of about 60 s or less. Imagine a very large shielded passive neutron detection array that can surround a vehicle, such as a tractor-trailer truck, on four sides and that is long enough for the entire vehicle to be inside the detection region. This configuration is similar to that proposed for some active interrogation and passive muon scattering approaches to vehicle inspection [58], sometimes referred to as a "nuclear car wash." A vehicle, or container, to be measured for neutron activity is placed inside the detector assembly and is counted for some time period. One concept configuration would be a neutron detector assembly with inside dimensions of 5 m wide by 5 m tall by 20 m long, surrounded by a steel box, as depicted in Fig. 15. This array consists of 320 detector panels of the typical polyethylene moderated neutron detection assembly with dimensions as defined above (0.62 m by 2.008 m).

Fig. 16 shows the absolute efficiency (number of detected neutrons divided by the number of emitted neutrons) for detection of an unmoderated $^{252}$Cf neutron source as a function of position within the detection system shown in Fig. 15. The upper schematic shows the individual source positions used in the calculations. The plots show the absolute efficiency with and without the surrounding iron box. The maximum efficiency is seen to be about 13% and occurs at the center.[5] This is close to the intrinsic efficiency since the solid angle of the detector for a source at the center is 96% of $4\pi$. This value is seen to be somewhat larger than the detection efficiency discussed in the previous section of a neutron hitting a two-tube detector assembly. This increase comes from the neutrons that are scattered into each detector assembly by neighboring assemblies, but the increase is relatively small since each assembly was already asymptotically approaching its maximum detection efficiency.[6] The efficiency drops to about half of the maximum for a source at the ends of the assembly.

The typical polyethylene moderated neutron detection assembly (0.62 m by 2.01 m) with a single tube has an observed background count rate of about 2–4 counts/s at the elevation and latitude of Pacific Northwest National Laboratory. This differs from the detection efficiency of ~10% computed above and the assumed average sea level neutron flux of ~100 neutrons/(s m$^2$). The reason derives from design differences between the modeled detector and

[5]Maximum values are 12.4% without the iron, and 12.8% with the iron outer box.

[6]Adding the four nearest neighbors to any detector increases its efficiency by about 11%. Adding all the detectors in the assembly increases a single detector's efficiency by about 25% due to the added reflected neutrons.

the actual detectors used for these measurements. For this model discussion, a background count rate of 10 counts/s will be assumed. An array of 320 detector panels is thus expected to have a background ($B$) of about 3200 counts/s. At the absolute detection efficiency found above of 13% for neutrons emitted from the centered source, and assuming no losses to neutron absorption in the cargo (a very optimistic assumption), the signal detected would then be about 13 counts/s from 25 kg of 90% enriched HEU (using the 97 neutrons/s value derived previously). Assuming Poisson statistics, the standard deviation in the background counts for a one second measurement would then be 57 counts, about four times the signal size for this time period. To obtain a three standard deviation ($\sigma$) measurement from the 13 count/s signal ($S$), a counting time of about 180 s would be required.[7] Such measurement times are perhaps possible for routine port operations using measurements where a vehicle stops inside the detector ("wait-in," as opposed to drive-through measurement). The feasibility of detecting a source that is shielded by certain cargo will generally be more difficult and will depend on the specific scenario.

However, a potential problem with any approach to measuring neutrons is the increased neutron backgrounds produced by the ship effect. Experience has shown that a three standard deviation measurement is probably inadequate for a definitive determination of the presence of a neutron source due to the sporadic nature of the neutron background, including the ship effect. The different time structure of neutrons emitted from a local neutron source versus ship effect neutrons, which tend to come in bursts, may allow this background to be eliminated. Since cosmic-ray produced neutrons are part of an air shower, surrounding the detector with a cosmic ray anticoincidence detector might be used to veto some ship effect events.[8] Experimentation on some of these questions is underway and the results will be reported in a later paper.

Assuming ship effect backgrounds can be reduced, it may be operationally feasible to perform targeted inspections that are 60 s or longer. This would possibly allow the detection of smaller quantities of shielded HEU. Passive neutron detection of fractions of a significant quantity of HEU may then become feasible with longer counting times if ship effect backgrounds can be vetoed. As discussed earlier, the neutron background varies with location, and thus some sites may have more or less background than assumed in this example, though most deployed systems are near sea level.

The practicality of any large passive or active detection system will require a careful analysis of the feasibility in an operational environment, the benefit obtained, and the cost. The anticipated cost of implementing the conceptual large passive neutron detection system discussed here, using existing commercial components, is likely to be significant, but comparable to a muon scattering system [60], and probably less than that of an active interrogation system. Further research on any such concept is required.

[7] From $\sigma = St/\sqrt{Bt}$, where $\sigma$ is the standard deviation, $S$ is the signal count rate, $B$ is the background count rate, and $t$ is the measurement time.

[8] A recent paper by Heimbach describes measurements of muon–neutron coincidences, and finds no measurable coincidence rate [59]. While this may indicate anticoincidence detectors may not be effective, investigation for the application described here would need to be made.

## 10. Summary and conclusions

Neutron detectors are complementary to gamma-ray detectors as part of passive monitoring systems, such as RPMs, for border interdiction applications. Because of the relatively small neutron emission rate from HEU, the role of neutron detectors in currently deployed systems is essentially for plutonium interdiction, for which the neutron signature is significant. However, factors that significantly affect passive gamma screening for special nuclear material for border applications, such as background radiation effects and nuisance alarms from commercial sources, are of much less concern for passive neutron screening. Motivated by these apparent advantages, the capabilities and limitations of a typically deployed $^3$He-tube-based detector assembly have been examined through simulation. In particular, the effects of cargo materials on emissions from neutron sources and the effects of moderation on detection efficiency have been demonstrated. Based on these modeling results, it was shown that it may be feasible to deploy a large array of passive neutron detectors that could be used to detect significant quantities of HEU under a number of scenarios. The key to the feasibility of such a system will be the ability to manage the impact of neutron backgrounds.

## Acknowledgments

This work was supported by the United States Department of Homeland Security. Pacific Northwest National Laboratory is operated for the United States Department of Energy by Battelle under Contract DE-AC05-76RLO 1830, PNNL-SA-54753, PIET-43714-TM-634. The Newark Neutron Monitor data are provided by The Bartol Research Institute neutron monitor program supported by the United States National Science Foundation under Grant ATM-0527878.

## References

[1] R.T. Kouzes, Am. Scientist 93 (2005) 422.
[2] P.E. Fehlau, C. Garcia Jr., R.A. Payne, E.R. Shunk, Vehicle monitors for domestic perimeter safeguards, Los Alamos National Laboratory, LA-9633-MS UC-15, January 1983.
[3] A. Clouvas, S. Xanthos, G. Takoudis, C. Potiriadis, J. Silva, Health Phys. 88 (2) (2005) 154.
[4] R.T. Kouzes, Public protection from nuclear, chemical, and biological terrorism, in: A. Brodsky, R.H. Johnson Jr. (Eds.), The 2004 Health Physics Society Summer School, Medical Physics Publishing, Madison, WI, 2004, pp. 31–46.

[5] R.C. Byrd, J.M. Moss, W.C. Priedhorsky, C.A. Pura, G.W. Richter, K.J. Saeger, W. Robert Scarlett, S.C. Scott, R.L. Wagner Jr., IEEE Sensors J. 5 (4) (2005) 593.
[6] R.T. Kouzes, J.H. Ely, J. Evans, W. Hensley, E.A. Lepel, J. McDonald, J.E. Schweppe, E.R. Siciliano, D. Strom, M. Woodring, Transport Storage Security Radioactive Mater. 17 (1) (2006) 11.
[7] J.H. Ely, R.T. Kouzes, J.E. Schweppe, E.R. Siciliano, D. Strachan, D.R. Weier, Nucl. Instr. and Meth. A 560 (2006) 373.
[8] R.T. Kouzes, E.R. Siciliano, Radiat. Meas. 41 (2006) 499.
[9] C.A. LoPresti, D.R. Weier, R.T. Kouzes, J.E. Schweppe, Nucl. Instr. and Meth. A 562 (2006) 281.
[11] J.L. Jones, W.Y. Yoon, D.R. Norman, K.J. Haskell, J.M. Zabriskie, S.M. Watson, J.W. Sterbentz, Nucl. Instr. and Meth. B 241 (2005) 770.
[12] K.A. Jordan, T. Gozani, Detection of 235U in hydrogenous cargo with differential die-away analysis and optimized neutron detectors, Nucl. Instr. and Meth A 579 (2007) 388.
[13] B.J. Micklich, D.L. Smith, Nucl. Instr. and Meth. B 241 (2005) 782.
[14] E.B. Norman, S.G. Prussin, R.-M. Larimer, H. Shugart, E. Brown, A.R. Smith, R.J. McDonald, H. Nitsche, P. Gupta, M.I. Frank, T.B. Gosnell, Nucl. Instr. and Meth. A 521 (2004) 608.
[15] D.R. Slaughter, M.R. Accatino, A. Bernstein, J.A. Church, M.A. Descalle, T.B. Gosnell, J.M. Hall, A. Loshak, D.R. Manatt, G.J. Mauger, T.L. Moore, E.B. Norman, B.A. Pohl, J.A. Pruet, D.C. Petersen, R.S. Walling, D.L. Weirup, S.G. Prussin, M. McDowell, Nucl. Instr. and Meth. B 241 (2005) 777.
[16] K.W. Geiger, L. Van der Zwan, Health Phys. 21 (1971) 120.
[17] International Organization for Standardization, Neutron reference radiations for calibrating neutron measuring devices used for radiation protection purposes and for determining their response as a function of neutron energy, Standard ISO/DIS 8529, Geneva, Switzerland, 1989.
[18] IAEA Safeguards Glossary 2001 Edition, International Verification Series No. 3, Table-II and paragraph 3.14, Vienna, Austria, 2002.
[19] H. Schraube, B. Hietel, J. Jakes, V. Mares, G. Schraube, E. Weitzenegger, Radiat. Prot. Dosim. 70 (1997) 337.
[20] Technical Reports Series No. 403, Compendium of Neutron Spectra and Detector Responses for Radiation Protection Purposes: Supplement to Technical Reports Series No. 318, International Atomic Energy Agency, Vienna, Austria, 2001.
[21] R.V. Griffith, Multi-technique characterization of neutron fields from moderated $^{252}$Cf and $^{238}$PuBe sources, National and International Standardization of Radiation Dosimetry (Proc. Symp. Atlanta, 1977), vol. 2, IAEA, Vienna, Austria, 1978, pp. 167–188.
[22] R.C. Runkle, T.M. Mercier, K.K. Anderson, D.K. Carlson, IEEE Trans. Nucl. Sci. NS-52 (6) (2005) 3020.
[23] G.F. Knoll, Radiation Detection and Measurement, third ed, Wiley, New York, 2002.
[24] A.J. Peurrung, Nucl. Instr. and Meth. A 443 (2000) 400.
[25] Z.W. Bell, G.M. Brown, C.H. Ho, F.V. Sloop Jr., Proc. SPIE 4784 (2002) 150.
[26] A. Syntfeld, M. Moszynski, R. Arlt, M. Balcerzyk, M. Kapusta, M. Majorov, R. Marcinkowski, P. Schotanus, M. Swoboda, D. Wolski, IEEE Trans. Nucl. Sci. NS-52 (6) (2005) 3131.
[27] M. Bliss, R.L. Brodzinski, R.A. Craig, B.D. Geelhood, M.A. Knopf, H.S. Miley, R.W. Perkins, P.L. Reeder, D.S. Sunberg, R.A. Warner, N.A. Wogman, SPIE 2551 (1995) 108.
[28] C.S. Blessinger, R.L. York, Neutron Detection Algorithm Development, Oak Ridge National Laboratory ORNL/TM-2006/157 (November 2006).
[29] American National Standard for Evaluation and Performance of Radiation Detection Portal Monitors for Use in Homeland Security, Technical Report, ANSI 42.35, American Nuclear Standards Institute, Washington, DC.
[30] F. Arneodo, A.B. di Tigliole, F. Cavanna, A. Cesana, Y. Chen, R. Dolfini, R. Nardo, G.P. Mortari, A. Rappoldi, G.L. Raselli, M. Rossella, C. Rossi, M. Tatananni, M. Terrani, Nuovo Cimento Soc. Ital. Fis. A 112 (1999) 819.
[31] J.W. Cronin, Rev. Mod. Phys. 71 (1999) S165.
[32] M.S. Gordon, P. Goldhagen, K.P. Rodbell, T.H. Zabel, H.H.K. Tang, J.M. Clem, P. Bailey, IEEE Trans. Nucl. Sci. NS- 52 (6) (2005) 2703 Part 1.
[33] R.J. Sheu, J.S. Lin, S.H. Jiang, Nucl. Instr. and Meth. A 476 (1–2) (2002) 74.
[34] B. Wiegel, A.V. Alvera, M. Matzke, U.J. Schrewe, J. Wittstock, Nucl. Instr. and Meth. A 476 (2002) 52.
[35] M. Yamashita, L.D. Stephens, H.W. Patterson, J. Geophys. Res. 71 (16) (1966) 3817.
[36] R.M. Lindstrom, D.J. Lindstrom, L.A. Slaback, J.K. Langland, Nucl. Instr. and Meth. A 299 (1990) 425.
[37] K. O'Brien, H.A. Sandmeier, G.E. Hansen, J.E. Campbell, J. Geophys. Res. Space Phys. 83 (Na1) (1978) 114.
[38] M.S. Gordon, P. Goldhagen, K.P. Rodbell, T.H. Zabel, H.H.K. Tang, J.M. Clem, P. Bailey, IEEE Trans. Nucl. Sci. NS- 51 (6) (2004) 3427.
[39] P. Goldhagen, Experimental study of the neutron "Ship Effect," Environmental Measurements Laboratory Annual Report—FY 2004, EML-625, 2005, pp. 9–10.
[40] H. Carmichael, Cosmic Rays (Instruments), in: C.M. Minnis (Ed.), Annals of the IQSY, Vol. 1: Geophysical Measurements, MIT Press, Cambridge, MA, 1968, pp. 178–197.
[41] S.E. Forbush, Phys. Rev. 51 (1937) 1108.
[42] R.P. Kane, Phys. Rev. 98 (1955) 130.
[43] C. Chung, C.Y. Chen, C.H. Kung, Appl. Radiat. Isot. 49 (4) (1998) 415.
[44] P. Goldhagen, M. Reginatto, T. Kniss, J.W. Wilson, R.C. Singleterry, I.W. Jones, W. Van Steveninck, Nucl. Instr. and Met. A 476 (1–2) (2002) 42.
[45] P. Goldhagen, J.M. Clem, J.W. Wilson, Radiat. Prot. Dosim. 110 (1–4) (2004) 387.
[46] R.A. August, G.W. Phillips, S.E. King, J.H. Cutchin, Nucl. Instr. and Meth. A 353 (1–3) (1994) 712.
[47] M.I. Frank, S.G. Prussin, P.F. Peterson, M.T. Tobin, J. Radioanal. Nucl. Chem. 249 (1) (2001) 145.
[48] D.L. Haggard, J.E. Tanner, G.M. Mapili, A. Mozhayev, A. Savlov, Proc. SPIE Int. Soc. Opt. Eng. 3536 (1999) 159.
[49] T.E. Kiess, Trans. Am. Nucl. Soc. 95 (2006) 9.
[50] M. Benedict, T.H. Pigford, H.W. Levi, Nuclear Chemical Engineering, second ed, McGraw-Hill, Inc., New York, 1981.
[51] MCNP X-5 Monte Carlo Team, MCNP—a general purpose Monte Carlo N-particle transport code, version 5, LA-UR-03-1987, Los Alamos National Laboratory, April 2003. The MCNP code can be obtained from the Radiation Safety Information Computational Center (RSICC), Oak Ridge, TN.
[52] W.B. Wilson, R.T. Perry, W.S. Charlton, T.A. Parish, G.P. Estes, T.H. Brown, E.D. Author, M. Bozoian, T.R. England, D.G. Madland, J.E. Stewart, SOURCES-4A: a code for calculating (alpha, n), spontaneous fission, and delayed neutron sources and spectra, Los Alamos National Laboratory Report LA-13639-MS, September 1999.
[53] "SYNTH: A computer code to generate synthetic Gamma-Ray Spectra," developed by The Pacific Northwest National Laboratory, Richland, WA, USA, with Government support under Contract Number DE-AC06-76RLO-1830 awarded by the United States Department of Energy. Copyright 1994–2006 Battelle Memorial Institute.
[54] J.E. Stewart, Principles of total neutron counting, in: Passive Nondestructive Assay of Nuclear Materials (PANDA), Nuclear Regulatory Commission NRC-FIN-A7241, 1991, pp. 407–434. Available at 〈www.nis5.lanl.gov/panda_manual.htm〉.
[55] D.M. Gilliam, A.K. Thompson, J.S. Nico, A neutron sensor for detection of nuclear material in transport, in: J.I. Trombka, et al. (Eds.), Unattended Radiation Sensor Systems for Remote Applications, American Institute of Physics 0-7354-0087-3, 2002.

[56] L.M. Wein, A.H. Wilkins, M. Baveja, S.E. Flynn, Preventing the importation of illicit nuclear materials in shipping containers. Risk Anal. 2007, to be published.
[57] L.M. Wein, Y. Liuy, Z. Caoz, S.E. Flynn, The optimal spatial deployment of radiation portal monitors can improve nuclear detection at ports. 2007, to be published..
[58] L.J. Schultz, K.N. Borozdin, J.J. Gomez, G.E. Hogan, J.A. McGill, C.L. Morris, W.C. Priedhorsky, A. Saunders, M.E. Teasdale, Nucl. Instr. and Meth. A 519 (2004) 687.
[59] C.R. Heimbach, J. Res. Natl. Inst. Stand. Technol. 112 (2007) 95.
[60] W.C. Priedhorsky, K.N. Borozdin, G.E. Hogan, C. Morris, A. Saunders, L.J. Schultz, M.E. Teasdale, Rev. Sci. Instrum. 74 (10) (2003) 4294.